FEATURE ARTICLE

Check for updates

Epitome of polyoxotungstate-coordinated lanthanide-based single-molecule magnets†

Pradip Kumar Sahu, ‡ Sandhya Kapurwan ‡ and Sanjit Konar *

Single-molecule magnets (SMMs) have garnered significant interest due to their possible use in high-density data storage devices and quantum computing. SMMs based on lanthanide-encapsulated polyoxotungstate (POT) have emerged due to their stability under ambient conditions and potential application in magnetic devices. The POTs can stabilize various anisotropic lanthanide ions (Ln(III)) with a range of strong to moderate ligand fields. The systematic combination of Ln(III) ions with POTs leads to significant perturbation in the electronic structure of the Ln(III) ion, which notably influences their magnetic properties. The magnetic properties of Ln(III)-POT clusters are highly dependent on the first coordination geometry and ligand field strength around the Ln(III) ions. Moreover, the bulky and diamagnetic POTs efficiently minimize the intermolecular magnetic interactions. As a result, the under-barrier magnetic relaxation is suppressed, and magnetic performance is enhanced. Over the years, a diverse array of Ln-POT SMMs have enriched the literature containing vacant POTs as building blocks (such as Keggin, Lindqvist, Wells–Dawson, and Preyssler types). In this review, we have discussed and summarized the effects of structural and bonding diversities of POTs on the SMM behaviour of Ln-POT clusters. This review aims to provide future direction and exploration of the challenging and compelling field of POT-based SMMs.

Introduction

Single-molecule magnets (SMMs) are paramagnetic metal complexes with the ability to block magnetization below a certain temperature (T_B), allowing them to retain magnetization for long periods and slowly demagnetize in the absence of a magnetic field.[1–4] They have potential applications in quantum computing, molecular spintronics, and high-density data storage, where each molecule can store magnetic information.[5–8] The lanthanide (Ln(III)) complexes are the most advantageous system due to their huge unquenched orbital angular momentum and inherent magnetic anisotropy, which is a crucial criterion for achieving high-performance SMMs.[9–12] By modulating the coordination

Department of Chemistry, IISER Bhopal, Bhauri, Bhopal by-pass road, Bhopal, Madhya Pradesh-462066, India. E-mail: skonar@iiserb.ac.in
† Electronic supplementary information (ESI) available. See DOI: https://doi.org/10.1039/d5cc00732a
‡ These authors contributed equally.

Pradip Kumar Sahu obtained his MSc in 2018 at the University of Hyderabad, India. In 2018, he joined the group of Prof. Sanjit Konar, IISER Bhopal, to carry out his doctoral research and earned his degree in 2024. His PhD research concentrated on the area of lanthanide metal-based high-performance single-molecule magnets (SMMs).

Pradip Kumar Sahu

Sandhya Kapurwan obtained her MSc in 2016 from HNB Garhwal University, India. In 2017, she joined the group of Prof. Sanjit Konar, IISER Bhopal, to carry out doctoral research and earned her degree in 2024. Her PhD project was focused on lanthanide single-molecule magnets (SMMs) using polyoxometalates (POMs).

Sandhya Kapurwan

geometry and symmetry around the metal center with the aid of an appropriate ligand field, the magnetic anisotropy of SMMs can be regulated.[13–20] However, to achieve the practical usefulness of SMM-based technology, the SMM should possess a high energy barrier for slow relaxation of magnetization (U_{eff}) and high blocking temperature (T_B), where U_{eff} refers to the effective energy barrier required for the conversion of a single-molecule magnet (SMM) into a paramagnetic state. This requires a substantially large anisotropy around the Ln(III) ion. Therefore, the presence of a strong axial coordination environment is the foremost requirement.[21–23] Several strategies have been employed to develop high-performance lanthanide-based single-molecule magnets, focusing on crystal field (CF) symmetry, predominant bonding interactions, organometallic frameworks, and strong magnetic coupling.[24–34] Along this line, many dysprosium metallocene cations were reported with T_B near the boiling point of liquid nitrogen (77 K).[23] Despite these advances, these SMMs are highly reactive to air and moisture. Thus, these molecules must be handled under an inert atmosphere. On the other hand, SMMs based on lanthanide-encapsulated polyoxometalates (Ln-POMs) offer a promising alternative due to their easy synthesis and exceptional stability under ambient conditions. Polyoxometalates (POMs) are anionic oxo-clusters of early transition metals in their high oxidation states, which provide aesthetical structural features as well as strong to moderate ligand field strength towards the metal ions.[35–39] They are effective multidentate building blocks for creating cluster complexes based on transition and lanthanide metals because of their strong negative charge and numerous oxo-donor sites.[40–47] POMs provide highly symmetric coordination sites toward Ln(III) ions while maintaining effective magnetic isolation and stability of Ln-POM clusters in both the solution and the solid state. The magnetic behaviour of Ln-POMs can be finely tuned, resulting in a wide range of magnetic phenomena, such as molecular spin frustration, electron delocalization-related properties, and SMMs.[48–54]

SMMs based on POMs can be classified into three families based on encapsulated metal ions: (a) POMs encapsulating transition metal ions,[55–60] (b) POMs encapsulating lanthanide ions,[61–64] and (c) POMs incorporating a mixed-valence POM cluster.[65–71] The beneficial properties of POMs have prompted great interest in the scientific community, leading to exponential growth in the number of publications over the last decade. POM clusters have been mainly reported with first-row transition metals (V, W, and Mo).[35,36,52] Among those POMs, polyoxotungstate (POT)-based metal ion encapsulated clusters mainly enrich the literature.[72–76] However, it should be noted that the formation of a POT cluster is not controllable during reaction. Recently, a few groups demonstrated the formation of various types of POMs using robotic machine learning methods.[77–81] In parallel, the inherent emerging nature of this lanthanide POM research field is expanding to new avenues, from materials design towards catalysis, to novel device fabrication, and to Qubits.[82–87]

This feature article provides a comprehensive overview of Ln(III) encapsulated polyoxotungstate-based molecules, focusing on their structural diversities. We categorized Ln-POTs based on their POM building units (Schemes 1, 2 and Table S1, ESI†). The bonding motif of these POM building units plays a crucial role in modulating the geometry around the first coordination sphere of the metal ions. This, in turn, influences the magnetic properties of Ln-POMs by altering the electronic behavior of the Ln(III) ions. In this feature article, we explore the coordinating geometry-dependent magnetic modulation phenomenon and highlight how structural variation affects the magnetic properties of these molecules.

Types of POMs and their synthetic strategies

The protonation of an oxometallate ion under controlled conditions (such as pH, concentration, and temperature) initiates the polycondensation of MO_4^{2-} units, forming complex polyanions known as polyoxometalates (POMs).[88–91] POMs are categorized into isopolyanions (IPAs) and heteropolyanions (HPAs).

Isopolyanions (IPAs). Isopolyoxoanions are polyoxometalates (POMs) with the general formula $[M_nO_{(4n-m)}]^{(2n-m)-}$ consisting of only one type of high-valent group V or VI transition metal ion, known as the addenda atom, and oxygen (O). IPAs, such as Anderson–Evans and Lindqvist structures, form through the condensation of similar species, with a degree of condensation greater than or equal to 6 ($n \geq 6$). They are often less stable than their heteropolyanion counterparts, but they offer unique physical properties, such as high charge densities and strongly basic oxygen surfaces, making them valuable as structural building blocks.

$$n[MO_4]^{2-} + 2m[H]^+ \leftrightarrow [M_nO_{(4n-m)}]^{(2n-m)-} + mH_2O$$
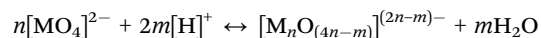
Heteropolyanions (HPAs). Heteropolyoxoanions are polyoxometalates (POMs) with the general formula $[X_xM_mO_y]^{n-}$, consisting primarily of one type of transition metal atom (M) in a high atomic proportion, along with a smaller proportion of other types of auxiliary atoms (X), known as heteroatoms (e.g.,

Sanjit Konar

Prof. Sanjit Konar received his PhD from the Indian Association for the Cultivation of Science, Kolkata. He worked as a postdoctoral fellow at the University of Notre Dame and Texas A&M University, College Station, TX, USA. He is a recipient of an Alexander von Humboldt Fellowship and has worked at Universität Bielefeld, Germany. Currently, he is working as a Professor at the Department of Chemistry, IISER Bhopal. His research interests are in single-molecule magnets and switchable magnetic materials. He has published 160+ peer-reviewed journal articles.
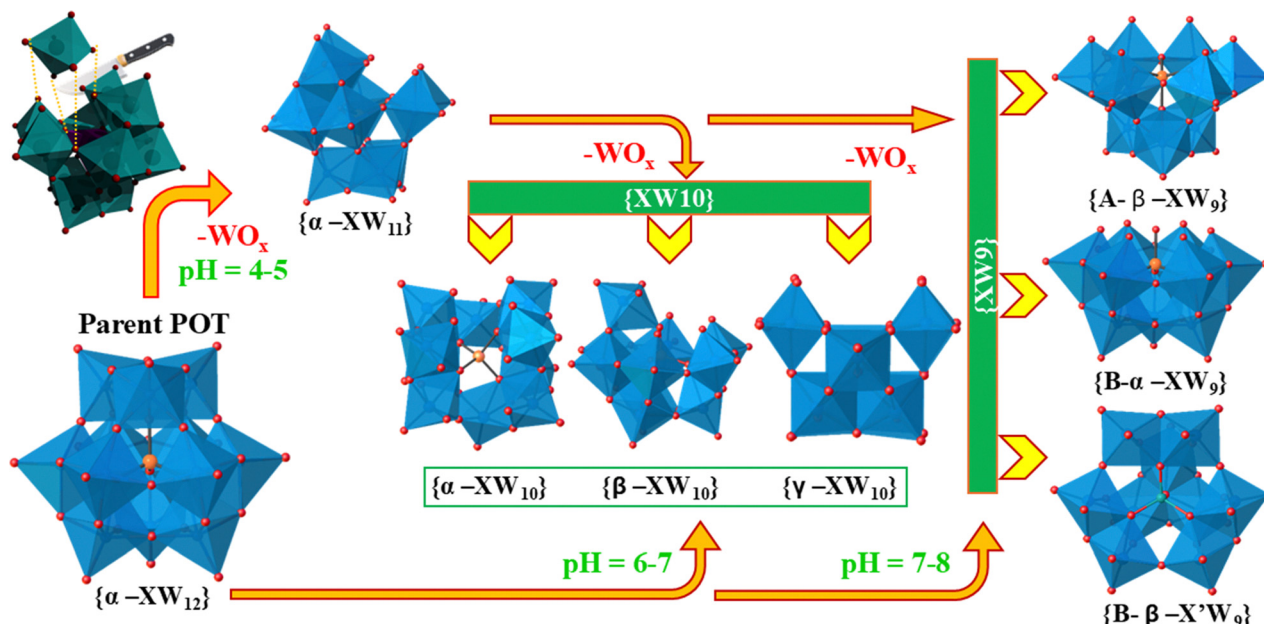
Scheme 1 Diverse structural motifs of polyoxotungstates formed by modulating the pH of the reaction medium (shown in the bottom arrows). Color code: blue polyhedral WO6, red O, orange P/Si. X = P, As, Si.

Si, P, As, Ge) or another metal atom. This subset of POM clusters is extensively studied, with particular focus on well-known examples such as the archetypal Keggin $[XM_{12}O_4]^{n-}$ (X/M = 1/12) and Wells–Dawson $[X_2M_{18}O_{62}]^{n-}$ anions (X/M = 2/18) (where M = W or Mo; X is a tetrahedral template).

$$12[WO_4]^{2-} + [HPO_4]^{2-} + 23[H]^+ \rightarrow [PW_{12}O_{40}]^{3-} + 12H_2O$$
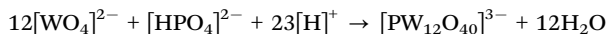
Among all the POM clusters, tungsten-based POMs are robust, and this fact has been exploited to develop tungsten-based Keggin and Dawson anions with vacancies known as lacunary polyoxotungstates (Scheme 1). These lacunary POMs are produced by controlled treatment of polyoxotungstate species with a base, resulting in the removal of one or two MO units from fully occupied POMs like $[XW_{12}^{VI}O_{40}]^{n-}$, leading to
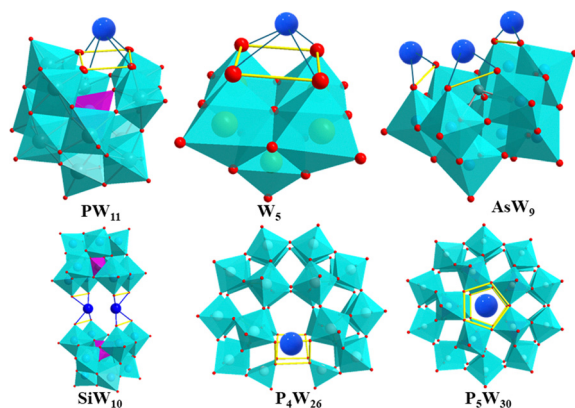
mono, di, and tri-lacunary forms such as $[XM_{11}O_{39}]^{n-}$, $[XM_{10}O_{36}]^{n-}$, and $[XM_9O_{34}]^{n-}$. The incorporation of heteroatoms with stereoactive lone pairs of electrons further enhances their versatility. The lone pair in the precursor molecule plays a crucial role in directing the self-assembly process, facilitating the formation of larger and more complex structures upon reaction with electrophiles. The coordination of Ln(III) cations with POM units to prepare Ln-POMs can be achieved through two main methods: one-pot synthesis and the building block method.

One-pot synthesis of Ln-POMs. This method involves the condensation of metal salts of building units and lanthanide ions with heteroanions, offering a straightforward yet highly tunable approach to synthesis. However, achieving the desired structures necessitates precise control over key synthetic parameters, including the molar ratios of reactants, pH, temperature, and solvent composition. Among these factors, pH is particularly crucial for obtaining specific structures. Various lanthanide polyoxometalates (Ln-POMs) have been synthesized through self-assembly by using stoichiometric quantities of the elements. In these processes, the equilibrium constants and formation rates are adequate for the polyanions to crystallize from acidified solutions at room temperature. The one-pot synthesis of Ln-POMs has proven to be an exceptionally efficient strategy, enabling the construction of diverse clusters while allowing the incorporation of various functionalities. As a result, this method remains the predominant route for the synthesis of Ln-POMs, as widely reported in the literature.

Building block method for Ln-POMs. This method employs lacunary POMs as reaction materials, utilizing the ligand-directing effect of oxygen to synthesize POM-based lanthanide oxo clusters (LnOCs). Numerous simple, high-yield synthetic

Scheme 2 Diverse binding motifs of different polyoxotungstates (POTs) with Ln(III) ions. Color code: light blue octahedron {WO6}, blue sphere Ln(III), red O, pink P/Si.

methods for lacunary POMs have been reported, allowing precise control over ligand-to-metal ion ratios, enhancing atomic utilization, and increasing synthetic success. As a result, lacunary POMs are widely used as efficient precursors, with nearly half of reported POM-based LnOCs, particularly pure 4f clusters, synthesized through this approach. These lacunary POM building units are highly sensitive to pH and other reaction conditions, leading to their potential decomposition or reconstruction in response to environmental changes during the reaction. Additionally, lacunary POMs can react with inorganic anions such as CO_3^{2-}, WO_4^{2-}, and PO_4^{3-}. These anions can serve as templates during the synthesis process, ultimately forming new building units. Trilacunary POMs, including both Keggin-type and Dawson-type, are frequently used due to their nucleophilic oxygen centers that act as excellent multidentate ligands. These POMs effectively coordinate with high-valency lanthanide ions, forming discrete LnPOMs or extended polymeric networks in one-dimensional (1D), two-dimensional (2D), and three-dimensional (3D) structures. This building-block strategy ensures controlled assembly and structural precision, facilitating the synthesis of highly symmetric Ln-POM clusters.

Significance of POMs as a ligand

In the literature, Ln-SMMs are mainly reported with organic ligands. POMs as an inorganic ligand towards Ln(III) ions are less explored due to their uncontrolled synthetic pathways. However, POMs offer significant advantages over organic ligands. This includes-

(a) Lacunary POMs can act as a multidentate ligand with the Ln(III) ion localized in the lacuna site (Scheme 2). Furthermore, the lacuna sites can be modified by synthetic modification, which provides various kinds of binding affinity towards the Ln(III) ion through oxo bridging sites.

(b) POMs are larger in size compared to organic ligands. They are rigid and diamagnetic also. This suppresses the intermolecular magnetic interactions in the crystal lattice.

(c) Moreover, it is possible to create clusters with a greater number of nuclei by manipulating specific chemical factors such as stoichiometry and pH. This property enables the control of both the number of nuclei and the specific type of magnetic interactions between various ions, thereby achieving a chosen spin ground state.

Types of POT building units used for SMMs

W$_5$-based SMMs. The SMM behavior in lanthanide-based magnets primarily depends on the geometry of the first coordination sphere.[12,13] The first studied Ln(III)-based SMM molecules contain a phthalocyaninato ligand.[2] Thus, many researchers use the {W$_5$} unit with lanthanide ions (Ln(III)) as $[W_5O_{18}]^{6-}$ have almost similar geometry and binding affinity towards Ln(III) ions.[92–94] The first Ln(III)-encapsulated SMM molecule, $[ErW_{10}O_{36}]^{9-}$, was reported by Coronado and coworkers.[92] This molecule shows a very narrow distribution of magnetic relaxation time due to the almost ideal D_{4d} ligand field symmetry around the Er(III) ion (Fig. 1). The simultaneous fitting of ligand field (LF) terms provided high negative axial LF terms. Thus, the
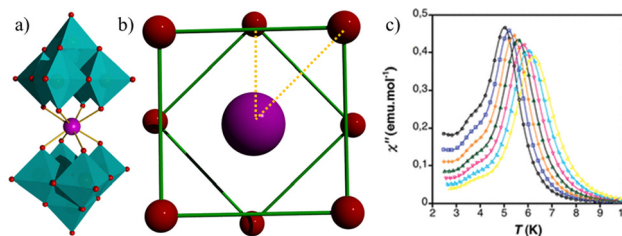

Fig. 1 (a) The molecular structure of $[ErW_{10}O_{36}]^{9-}$, (b) the symmetry around the Er(III) ion, and (c) out-of-phase magnetic susceptibility plot of the complex. Color code: cyan octahedron {WO$_6$}, red O, violet Er. Figure reprinted (adapted) with permission from ref. 92. Copyright (2008) American Chemical Society.

molecule showed a 55.2 K energy barrier. The modulation of magnetic relaxation of $[ErW_{10}O_{36}]^{9-}$ was studied upon its solvation and desolvation processes.[94] The solvated molecule showed a 51.8 K energy barrier, which is close to the energy difference between the ground and the first excited state. In contrast, the desolvated molecule follows the QTM relaxation process with an out-of-phase magnetic susceptibility peak at a high-frequency region ($\approx 10^4$ Hz). The molecule's magnetic relaxation behaviour is partially recovered on resolution. The solvated molecule shows an open hysteresis loop with a 1.375 kOe coercive field at 2 K. After desolvation, the hysteresis loop gets closed, which indicates that the in-field memory effect was annihilated in the desolvation process. The butterfly nature of the hysteresis loop reappears on resolution.

W$_9$-based SMMs. Lanthanide and transition metal ion encapsulation is best accomplished using the lacunary POM building block $[(XO_m)W_9O_{30}]^{6-}$ {X = P, Si, Sb, and As}.[95–102] This fragment unit can be formed via the dissociation of the Dawson-W$_{18}$ unit at acidic pH. Thus, designing the metal oxo clusters is challenging by conventional one-pot synthesis using the metal and {W$_9$}-polyoxo anions. In 2015, A. K. Powell and coworkers revealed that systematic K$^+$ ion concentration modulates the cationic-directed 3d–4f complex.[95] They performed step-by-step synthetic preparation to synthesize many 3d–4f complexes having GeW$_9$ building units. Out of those, only the Co-Dy ($[Dy_{30}Co_8Ge_{12}W_{108}O_{408}(OH)_{42}(OH_2)_{30}]^{56-}$) complex shows field-induced SMM behavior at zero field until 8 K (Fig. 2). The molecule contains three different types of Dy(III) ions regarding their coordination geometry. Due to this, the overall anisotropy of the molecule becomes less. As a result, magnetic relaxation mainly occurs through the QTM relaxation process (Fig. 2b and c). The application of the external DC field did not affect the involvement of the QTM relaxation process in the magnetic relaxation dynamics of the Co-Dy complex. Recently, Y. Huo and coworkers also demonstrated the formation of polynuclear Dy(III)-POT clusters by varying the pH of the reaction medium.[96] Due to the presence of various coordination environments around the Dy(III) ions, the molecules did not show significant frequency-dependent AC susceptibility data. In a later study, the pH of the reaction medium was changed with the help of different alkaline hydroxide solutions to regulate the assembly of the {α-AsW$_9$}$^{9-}$ clusters with Ln(III) ions (Fig. 3).[43] Along this line, M.-L. Tong and coworkers reported the formation
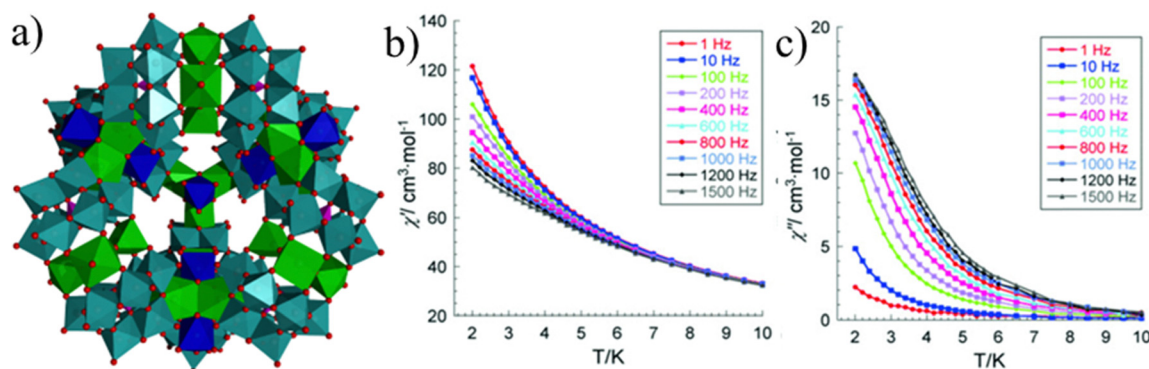
Fig. 2 The molecular structure of the $[Dy_{30}Co_8Ge_{12}W_{108}O_{408}(OH)_{42}(OH_2)_{30}]^{56-}$ molecule (a), and the temperature-dependent in-phase (b) and out-of-phase (c) magnetic susceptibility plot at zero DC field of the complex. Color code: cyan octahedron $\{WO_6\}$, green polyhedron Dy unit, blue polyhedron Co unit. Hydrogen atoms are omitted for clarity. Figures adapted from ref. 95, with permission from Wiley, copyright 2015.

of a highly symmetric Dy(III)-based hexanuclear molecule, $[K \subset \{(AsW_9O_{33})Dy(H_2O)_2\}_6]^{35-}$ at high pH of the reaction medium (Fig. 3b).[101] The six $\{AsW_9\}^{9-}$ units assembled like an idealized S_6 symmetrical molecule with an encapsulated K^+ ion inside the cavity and the assembled $\{AsW_9\}^{9-}$ unit provides bi-augmented trigonal prismatic symmetry around the Dy(III) ions. The AC magnetic susceptibility measurement shows the SMM nature of the complex under zero and 3000 Oe applied field. A thermal energy barrier of 68 K was obtained by applying a 3000 Oe external magnetic field (Fig. 3d). The low-temperature photoluminescence data further confirmed the similar energy separation between the ground and the first excited states. Later, our group reported the hexanuclear assemblies of various Ln-ions (Ln = Er, Tb, Gd, Ho) at

higher pH conditions.[102] The hexagonal arrangement of the lanthanide and $\{AsW_9\}$ unit provides C_{2v} symmetry around the Ln(III) ions. As a result, the energy states become a mixture of the m_J states, and non-axial energy terms become predominant (obtained from *ab initio* calculations). Only the Er-analog shows field-induced single-molecule magnet behaviour at 1500 Oe applied dc field. We further illustrated the formation of Ln-{α-$AsW_9\}^{9-}$ clusters by reducing the reaction medium's pH. This provides Cs^+ ion encapsulated tetra nuclear $[Cs \subset \{Ln_4(H_2O)_8 (\alpha-AsW_9O_{33})_4\}]^{23-}$ molecules (Ln = Dy, Tb).[97] The Tb(III) analogue of the molecule demonstrated the first SMM behaviour of the Tb(III) encapsulated $\{AsW_9\}^{9-}$-based molecule, $[\{Tb_4(H_2O)_8 (\alpha-AsW_9O_{33})_4\}]^{24-}$ (Fig. 3c). The Tb(III) ion is coordinated with
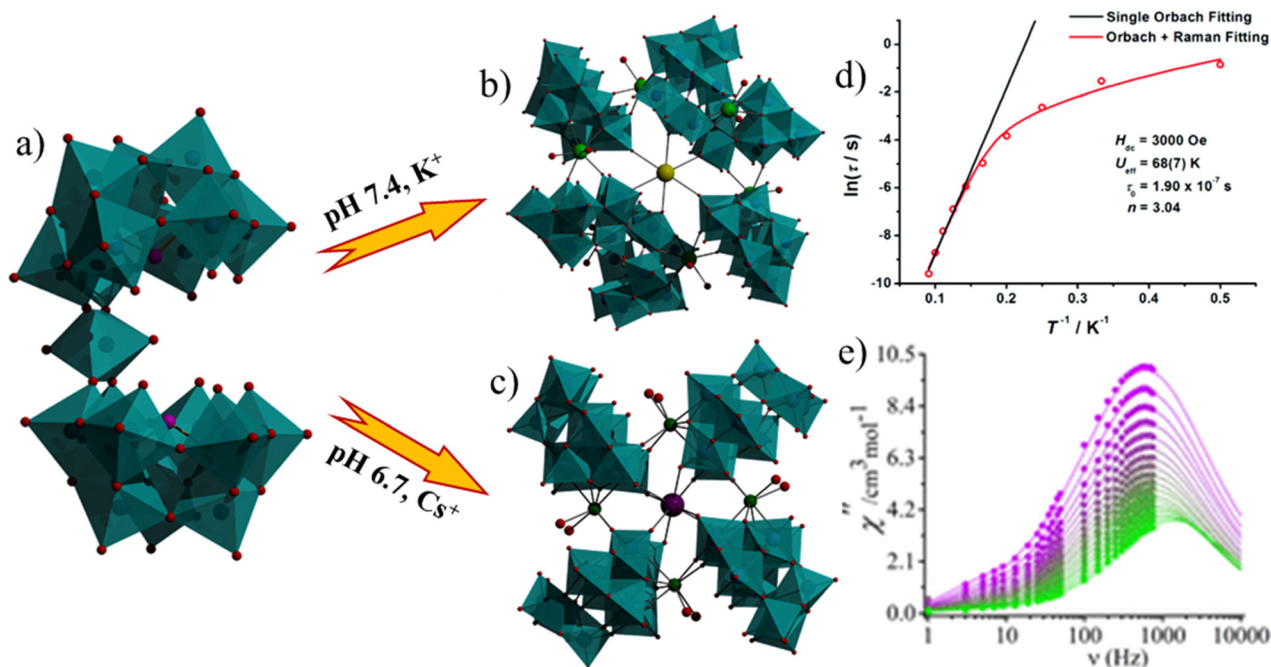

Fig. 3 The reaction conditions for the formation of $[K \subset \{(AsW_9O_{33})Dy(H_2O)_2\}_6]^{35-}$ (b) and $[Cs \subset \{Tb_4(H_2O)_8(\alpha-AsW_9O_{33})_4\}]^{23-}$ (c) from $[As_2W_{19}O_{67}(H_2O)]^{14-}$ (a) and their corresponding magnetic relaxation plot (d) and frequency-dependent out-of-phase magnetic susceptibility plot (e). Color code: cyan octahedron $\{WO_6\}$, green Dy, red O, yellow K, violet Cs, pink As. Hydrogen atoms are omitted for clarity. Figures reprinted (adapted) with permission from ref. 97 and 101. Copyright (2022) American Chemical Society, and (2017) Royal Society of Chemistry, respectively.

two Keggin POTs with terminal and epical oxygen atoms. The pseudo-C_{2v} geometry was satisfied by the presence of six oxides of two POTs and two oxygen atoms of coordinated water molecules. The local symmetry around the Tb(III) ion stabilizes the higher m_J state ($m_J = 6$). The molecule shows out-of-phase magnetic susceptibility maxima in the higher frequency region and shifts with increasing temperature (Fig. 3e). As a result, the molecule shows a phenomenological energy barrier of 15 K. The Dy analog of this previously mentioned complex also possesses the ground state with mixed m_J states. The magnetic relaxation of this molecule possesses shortcut relaxation dynamics with a thermal energy barrier of 24 K. Furthermore, it was proven by *ab initio* calculation that the presence of less transverse anisotropy and a high axial ground state mainly causes the SMM behaviour of these complexes. We have also demonstrated the SMM behaviour of both prolate and oblate Ln(III) ions in an oxalis triangularis assembly of $[(AsW_9O_{33})_3Ln_2(H_2O)_7W_4O_9]^{15-}$.[99] Using dilacunary arsenotungstate $[As_2W_{19}O_{67}(H_2O)]^{14-}$ as a precursor with Ln(III) ions, we have tuned the coordination symmetry of both prolate Dy(III) and oblate Yb(III) ion toward the intermediate of high and low axial symmetry. The Dy(III) analog shows zero-field SMM behaviour with the involvement of only the QTM relaxation process. Upon applying the 2000 Oe dc field, the molecules show a 56.48 K thermal energy barrier, whereas the Yb(III) analog shows field-induced SMM behaviour. Upon 2000 Oe applied dc field, it shows a 6 K phenomenological energy barrier. The intermediate symmetry stabilizes the axial ground states for Dy(III) ions and easy plane anisotropy for Yb(III) ions.

W_{10}-based SMMs. When two adjacent triads of an α-Keggin anion are rotated by 60°, the pair of edge-shared octahedra become unstable and are prone to dissociation under basic hydrolysis, resulting in the formation of di-vacant γ-$[XW_{10}O_{36}]^{n-}$ (γ-XW_{10}, X = Si^{IV}, Ge^{IV}, and P^V). Lacunary sites in the polyoxometalate (POM) building units act as flexible and variable coordination ligands, accommodating diverse geometries and numbers of metal cores.[103–106]

Previous studies have demonstrated that bridging structures between two metal cations in silicodecatungstate can be transformed through chemical stimuli.[107–110] This ability of POM ligands opens up the possibility of reversibly controlling SMM behavior. In this regard, Mizuno and co-workers reported reversible switching of SMM behavior by structural transformation of a dinuclear Dy-core in heteropolyoxotungstate $[\{Dy(H_2O)_2(CH_3COCH_3)\}_2(\gamma\text{-}SiW_{10}O_{36})_2]^{10-}$ (complex **1**) to $[Dy_2(\mu_2\text{-}OH)_2(\gamma\text{-}SiW_{10}O_{36})_2]^{12-}$ (complex **2**) upon addition of tetra-*n*-butyl ammonium hydroxide (TBAOH), which promotes hydrolysis of the H$_2$O ligand (Fig. 4a and b).[107] The AC susceptibility data for complex **2** indicate slow magnetic relaxation behavior with an effective energy barrier of 65.7 K, whereas complex **1** hardly shows SMM behavior (Fig. 4a and b). This change is attributed to the alteration in coordination geometry, which reduces repulsive contacts between ligands and the f-orbital electron density of dysprosium cations, thereby increasing the magnetic anisotropy of the Dy(III) ion.

Furthermore, the effect of the ionic radius of the Ln(III) center adjacent to the Dy(III) ion in the dinuclear core of complex **2** was investigated by synthesizing hetero-dinuclear
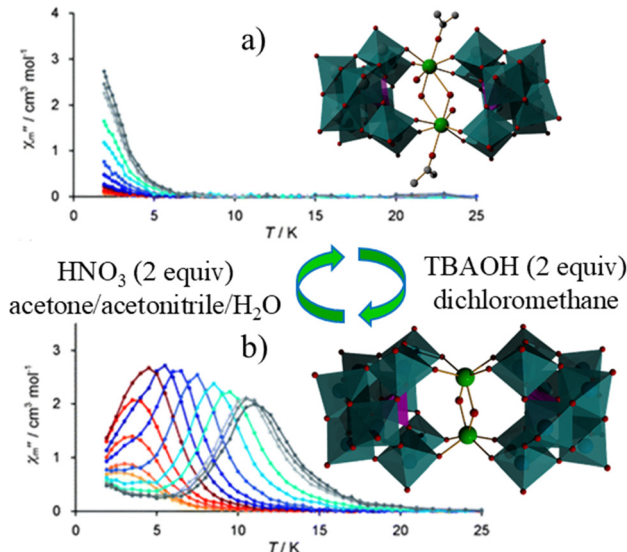

Fig. 4 The molecular structure and out-of-phase magnetic susceptibility of $[\{Dy(H_2O)_2(CH_3COCH_3)\}_2(\gamma\text{-}SiW_{10}O_{36})_2]^{10-}$ (a) to $[Dy_2(\mu_2\text{-}OH)_2(\gamma\text{-}SiW_{10}O_{36})_2]^{12-}$ (b) with their reaction conditions for reversible transformation. Color code: cyan octahedron {WO$_6$}, green Dy, red O, grey C. Hydrogen atoms are omitted for clarity. Pictures reproduced from ref. 107 with permission from the Royal Society of Chemistry.

lanthanide-containing POTs $[\{Ln(\mu_2\text{-}OH)_2Ln'\}(\gamma\text{-}SiW_{10}O_{36})_2]^{12-}$ (LnLn'; Ln = Dy; Ln' = Dy, Eu, Yb, Lu) through stepwise incorporation of Ln(III) ions into vacant sites of lacunary POMs.[108] AC susceptibility measurements showed that all complexes exhibit slow relaxation of magnetization, with the magnetization barrier increasing in the order: DyLu < DyYb < DyDy < DyEu. This is due to the elongation of the bond distance of bridging oxygen and DyLn', which enhances the magnetic anisotropy of the Dy(III) ion and the energy barrier for magnetization reversal. The $[GeW_{10}O_{38}]^{10-}$ building unit has also been utilized to synthesize large clusters, such as $[(H_2O)_6 \subset Dy_{12}(H_2O)_{24}(GeW_{10}O_{38})_6]^{36-}$ and $[(GeW_{10}O_{38})_6(Dy_{14}(H_2O)W_8(OH)O_{30})]^{43-}$, where it coordinates through different vacant sites.[109,110] However, the frequency-dependent AC signals are too weak for a meaningful fitting analysis. This is due to the diverse and complex coordination geometries of the crystallographically independent Dy(III) ions, which result in multiple magnetization relaxation processes.

W_{11}-based SMMs. The formation of $[SiW_{11}O_{39}]^{8-}$ {W_{11}} building units is highly dependent on the pH of the reaction medium.[111,112] In the lower pH range (especially between pH 3–4), the formation of {W_{11}} is more favourable. Thus, by maintaining the pH within this range, numerous lanthanide-based POM clusters have been successfully synthesized.[113–116] In 2019, M.-L. Tong and coworkers reported hydroxo and fluoride bridged dinuclear Dy(III) complexes, $[(PW_{11}O_{39})_2Dy_2X_2(H_2O)_2]^{10-}$ (X = OH, F).[116] The coordination geometry of Dy(III) in both complexes remains as capped trigonal prismatic (Fig. 5a and c). However, the magnetic relaxation behaviour largely depends on the ligand field strength. Having more electronegative F$^-$ ions in the bridging position lessens the axial anisotropy of the Dy(III) ions. The intra
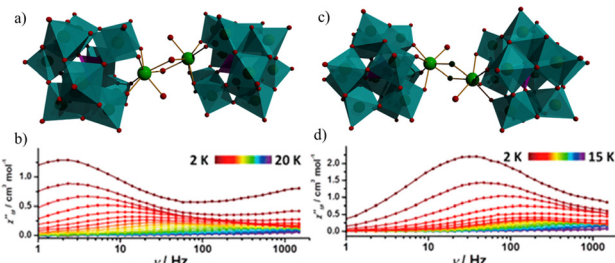
Fig. 5 The molecular structure of $[(PW_{11}O_{39})_2Dy_2X_2(H_2O)_2]^{10-}$ [X = OH (a), F (c)] and the frequency-dependent out-of-phase magnetic susceptibility plots of the respective complexes (b and d). Color code: cyan octahedron {WO_6}, green Dy, red O, deep green F. Hydrogen atoms are omitted for clarity. Figures reprinted (adapted) with permission from ref. 116. Copyright (2019) American Chemical Society.

Fig. 6 The molecular structure (a) and magnetic hysteresis plot (b) of $[LnW_{30}O_{110}]^{12-}$. Color code: cyan octahedron {WO_6}, green Dy. Figure reprinted (adapted) with permission from ref. 126. Copyright (2012) American Chemical Society.

and intermolecular Dy···Dy distance is greater for the bridged complex, and as a result, undesired intermolecular magnetic interaction is prevented. The AC magnetic susceptibility data shows SMM behaviour for both complexes at zero applied DC field (Fig. 5b and d). The magnetic relaxation of the fluoride-bridged complex shows an effective energy barrier of 108 K, which is the highest for fluoro-bridged POM-based SMMs. The *ab initio* calculation predicts that the energy separation between the ground and excited state is 84 and 104 cm^{-1} for the –F and –OH bridged complex, which was further confirmed by a low-temperature photoluminescence study. The magnetic axes are more parallelly orientated for the –OH bridged complex; as a result, it provides the highest energy barrier (U_{eff} = 141 K) for POM-based SMMs. Later, E. Coronado and coworkers reported a series of $[Ln(\beta_2\text{-}SiW_{11}O_{39})_2]^{13-}$ complexes [Ln = Tb(III)–Yb(III)].[113] The first coordination sphere around the Ln(III) ion is significantly distorted from D_{4d} symmetry, which was found in $[Ln(W_5O_{18})_2]^{9-}$. Besides this, the planes of coordinated oxygen atoms are not parallel ($\approx 2.8°$ tilted). This difference in geometry affects the ligand field strength on Ln(III) ions, resulting in a change of magnetic properties between these two types of Ln(III) encapsulated clusters. The [LnSiW$_{11}$] clusters did not show any SMM behaviour. Later, U. Kortz and coworkers reported a series of Ln(III) encapsulated isomeric {GeW$_{11}$} POM units.[114] The two {GeW$_{11}$} units coordinated with Ln(III) in a distorted square antiprismatic geometry. The twist angle between the two square planes increases along the Ln(III) row. The isomerization happens ($\beta_2 > \alpha$) in post-Dy(III) ions due to lanthanide contraction destabilizing β_2–β_2 species. Only the Er(III) analog shows field-induced SMM behaviour with an energy barrier of 62.3 K.

Highnuclearity {W_n}-unit based SMMs

Magnetic polyoxometalates (POMs) can be categorized into two main families. The first consists of lacunary POMs, such as Keggin and Dawson types that encapsulate metal ions connected through oxo bridges, forming magnetic clusters with variable nuclearity and high symmetries. The second family includes larger POM clusters that encapsulate lanthanide ions, resulting in complexes where 4f-magnetic ions interact with the crystal field generated by the POM ligands. This interaction
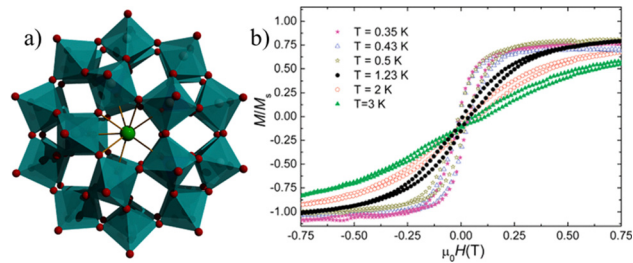
leads to various symmetries such as D_{2d}, D_{3h}, and C_∞, etc. Beyond the lacunary POM building blocks, these larger POM clusters offer significant advantages, including internal cavities that accommodate a range of metal cations, a high oxygen-rich surface, and exceptional stability across a broad pH range.[117–125] In 2012, Coronado and co-workers reported an interesting example, $[LnW_{30}O_{110}]^{12-}$ (Ln^{3+} = Dy, Ho), where {W_{30}} polyoxometalates act as a rigid ligand and are used for the design of metal complexes with very unusual C_5 axial symmetry.[126] Structural analysis revealed that Ln(III) ions occupy two identical coordination sites, leading to a mono-capped pentagonal antiprism geometry (Fig. 6a). Despite low symmetry around the Ln(III) centers, the SMM behavior was observed for both Dy and Ho derivatives with energy barrier U_{eff}/k_B = 24 K and $U_{eff}/k_B \approx 0.8$ K, along with hysteresis at low temperatures (Fig. 6b). More recently, P. Kögerler and coworkers reported solution-stable polyanions $[Na\{Ln(H_2O)\}\{WO(H_2O)\}P_4W_{26}O_{98}]^{12-}$ (Ln = Tb, Dy, Er, Ho, Tm, Yb), where Ln(III) is in a rare trigonal prismatic O_6 environment (Fig. 7a).[127] Structural analysis shows that in complex {P_4W_{26}}, two identical {P_2W_{12}} units connected through a μ_2-bridge by four oxygen atoms, which further coordinated with two W^{VI} ions through the open end of each {P_2W_{12}} building block and the central cavity of the {P_4W_{26}} entity is occupied by one W(VI) and Ln(III) ion (Ln = Sm–Lu). The Ln(III) ion exhibits nearly C_{2h}-symmetric trigonal prismatic coordination symmetry. The AC magnetic susceptibility measurements reveal field-induced (1000 Oe applied DC field) SMM behaviour of the Dy-analog with an
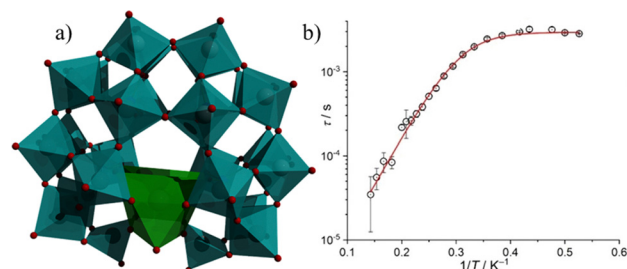

Fig. 7 The molecular structure (a) and magnetic relaxation plot (b) of $[\{Dy(H_2O)\}\{WO(H_2O)\}P_4W_{26}O_{98}]^{13-}$. Color code: cyan octahedron {WO_6}, green polyhedra Dy unit. Hydrogen atoms are omitted for clarity. Figures adapted from ref. 127, with permission from Wiley, copyright 2021.

energy barrier of 26 K (Fig. 7b). Furthermore, the impact of O–H vibration on magnetic relaxation was determined by an exchange of coordinated H_2O to Dy(III) by D_2O. The deuterated compound shows a 20% larger U_{eff} than the hydrated compound, which implies that the relaxation of the Ln(III) center is moderately affected by the vibrational mode of the water ligand.

Organic–inorganic POT-based SMMs

Organic–inorganic hybrids have garnered significant attention and made rapid strides in recent years by integrating unique properties of individual components into unified systems. Various types of polynuclear polyoxometalates (POMs), particularly dysprosium-based single-molecule magnets (Dy-SMMs), have emerged as high-performance examples.[128] These include organic–inorganic hybrid Ln-POMs incorporating carboxylates, organophosphates, amino acids, and other ligands, showcasing exceptional SMM behavior.

Organic–inorganic hybrid Ln-POMs can be divided into three broad families. The first class includes POMs encapsulating multiple Ln(III) ions connected by organic acids, ligands, or other POMs to form magnetic clusters with variable nuclearity and high symmetry.[129–133] A notable breakthrough in this field was achieved by C. Boskovic and co-workers through the use of POMs combined with organic acids as ligands. They reported a family of POT-ligated tetranuclear complexes, $[Ln_4As_5W_{40}O_{144}(H_2O)_{10}(L)_2]^{21-}$ (L = glycine acid), where the organic acid bridges two $\{As_2W_{19}O_{68}\}$ building units.[134] Those compounds were the first example of POM-supported polynuclear lanthanide-based SMMs, showcasing the potential of such hybrid materials. Later J. Wang and coworkers reported two tartaric acid bridged Ln-POT molecules, $[\{Dy(C_4H_2O_6)(\alpha\text{-}PW_{11}O_{39})\}_2]^{9-}$, where two mono-Dy substituted Keggin units were bridged by two organic tartaric acid ligands, resulting in eight coordinate highly distorted square antiprism geometries.[135] The frequency dependence of the ac-susceptibility suggested a typical single-molecule magnet (SMM) behavior with an energy barrier of 20 K. Furthermore, M.-L. Tong and coworkers reported $[\{(As\text{-}W_9O_{33})_3Dy_2(H_2O)_4W_4O_9(H_2O)\}_2(NH_2(CH_2PO_3)_2)]^{33-}$, utilizing organo-phosphonate ligands (Fig. 8a).[136] Structural analysis revealed two identical subunits connected by $\{NH_2(CH_2PO_3)_2\}$ ligands, with each phosphate group binding one W(VI) ion and one Dy(III) ion via P–O bonds. The magnetic measurements show nice frequency and temperature dependence of out-of-phase (χ'') ac susceptibility under zero field, indicating the slow relaxation of magnetization behavior. The linear fit of the Arrhenius equation results in an energy barrier to the spin reversal, U_{eff} = 99 K, and relaxation time, $\tau_0 = 1.16 \times 10^{-6}$ s (Fig. 8b). Additionally, the variable-temperature magnetization measurements show hysteresis up to 8 K. Nano-sized Dy-POM clusters, $[Dy_6(L)_4(H_2O)_{23}(ampH_2)(PW_{11}O_{39})_2]$ (complex 3) ($ampH_2$ = (aminomethyl)phosphonic acid) (pH = 2.9) and $[Dy_9(CO_3)_3(L)_2(H_2O)_{12}(PW_{10}O_{37})_6]^{35-}$ (complex 4) {L = (amino methyl)phosphonic acid ($ampH_2$)} (pH = 7.4) were reported by controlling the pH of the reaction mixture.[137] The structural analysis of complex 3 shows a hexanuclear Dy(III) core, sandwiched between
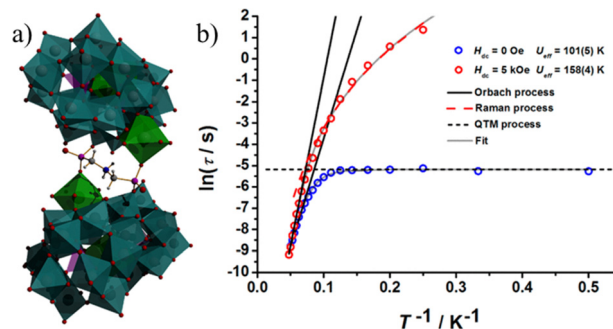

Fig. 8 The molecular structure (a) and magnetic relaxation plot (b) of $[\{(As\text{-}W_9O_{33})_3Dy_2(H_2O)_4W_4O_9(H_2O)\}_2(NH_2(CH_2PO_3)_2)]^{33-}$. Color code: cyan octahedron $\{WO_6\}$, green polyhedral Dy unit, red O, blue N, pink P, grey C, white H. Hydrogen atoms are omitted for clarity. Figure reprinted (adapted) with permission from ref. 136. Copyright (2017) American Chemical Society.

two $[PW_{11}O_{39}]^{7-}$ units, which are oriented at $180°$ to each other where the geometry around the Dy(III) centers is square antiprismatic. On the other hand, complex 4 consists of six $[PW_{10}O_{37}]^{9-}$ building blocks assembled around the $[Dy_9(CO_3)_3(ampH)_2(H_2O)_{12}]^{19+}$ ($\{Dy_9\}$) cluster core, which further consists of three $\{Dy_3\}$ units capped around two $ampH^-$ ligands where Dy(III) ions display distorted square antiprism geometry and capped trigonal prismatic geometry. The ac measurement reveals that only complex 4 shows zero field SMM behavior and magnetic hysteresis at 2 K.

Recently, M.-L. Tong and co-workers reported two Dy(III)–SMM complexes: $[Dy(OPPh_3)_4(H_2O)_3][PW_{12}O_{40}]$ (complex 5) and $[\{Dy(OPPh_3)_3(H_2O)_3\}\{PW_{12}O_{40}\}]$ (complex 6), utilizing the saturated Keggin-type polyoxoanion $[PW_{12}O_{40}]^{3-}$.[138] In these complexes, the Dy^{III} sites exhibit pseudo-pentagonal bipyramidal (PBP) symmetry with axial anisotropy provided by the strong axial Ph_3PO ligand. Magnetic studies reveal field-induced SMM behavior in complex 5, while complex 6 shows better SMM behavior, with an energy barrier of 310(7) K at zero field. Magneto-structural analysis shows that the enhancement in SMM behavior in complex 6 arises from replacing equatorial Ph_3PO with POM, which strengthens axial anisotropy. This provides a novel strategy for improving SMM behavior in lanthanide-based systems.

As double-decker-type complexes have shown great potential toward high-performance SMMs by harnessing single-ion anisotropy,[139–141] P. Kogerler and coworkers synthesized a Dy-double-decker complex, $[Dy^{III}Pc(PW_{11}O_{39})]^{6-}$ which comprises both Pc^{2-} and a mono lacunary α-Keggin $[PW_{11}O_{39}]^{7-}$ ligand (Fig. 9a).[142] Structural analysis shows that the Dy(III) ion coordinated to four oxygens of the lacunary site of $[PW_{11}O_{39}]^{7-}$ and the Pc^{2-} unit results in a distorted antiprismatic N_4O_4 geometry. Furthermore, the frequency and temperature dependence of the ac susceptibility data show the presence of slow magnetic relaxation with the spin reversal barrier of U_{eff} = 47.48 K and relaxation time of $\tau_0 = 1.08 \times 10^{-7}$ s (Fig. 9b). In the realm of organic–inorganic hybrid polyoxometalates (POMs), a second family features heterometallic 3d–4f compounds aimed at enhancing magnetic interactions and spin ground states.[130] A
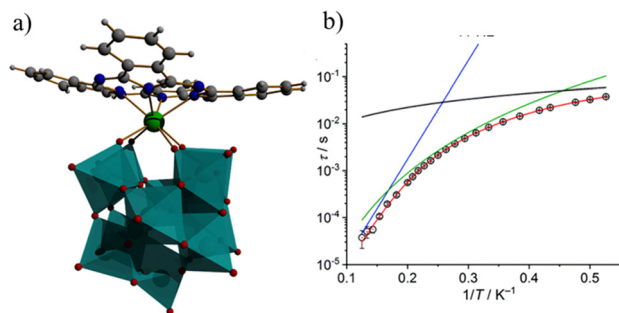
Fig. 9 The molecular structure (a), and the magnetic relaxation plot (b) of $[Dy^{III}Pc(PW_{11}O_{39})]^{6-}$. Color code: cyan octahedron $\{WO_6\}$, green Dy, grey C, blue N, white H. Picture reproduced from ref. 142 with permission from the Royal Society of Chemistry.

significant example was reported by Mizuno and co-workers, featuring 3d–3d′–4f heterotrimetallic heptanuclear clusters $[(A-\alpha-SiW_9O_{34})_2FeMn_4O_2\{Ln(acac)_2\}_2]$ (Ln = Gd^{3+}, Dy^{3+}, Lu^{3+}).[98] This involves the sequential introduction of metal cations into a trivacant lacunary POM $[A-\alpha-SiW_9O_{34}]^{6-}$, resulting in two $[Ln(L)_2]^+$ units at the ends of pentanuclear clusters $[FeMn_4O_{18}(OH)_2]^{23-}$ and $[FeCu_4O_{18}(OH)_2]^{27-}$. The addition of a third 4f ion significantly enhances magnetic interactions between $Mn^{3+}-Mn^{3+}$ ($J_2 = -9.51$ cm^{-1} for $FeMn_4Gd_2$; $J_2 = -7.10$ cm^{-1} for $FeMn_4Lu_2$). The AC magnetic susceptibility studies indicated that only the $FeMn_4Lu_2$ derivative exhibited typical single-molecule magnet (SMM) behavior with an effective energy barrier (U_{eff}) of 19.7 K. In 2019, S.-T. Zhang and co-workers reported novel Cr–Ln heterometallic clusters with the formula $[Cr_4Ln_4(\mu^4-O)_4(\mu^3-O)_4(C_8H_4O_4)_4-(H_2O)_{10}](H_6SiW_{12}O_{40})-Cl_2$ featuring prismatic $[Cr_4Ln_4]$ cores stabilized by organic ligands and inorganic POM species.[143] The magnetic investigation reveals the coexistence of ferromagnetic and antiferromagnetic couplings within the Cr_4Dy_4 core. The complexes did not show well-defined out-of-phase magnetic susceptibility (χ'') maxima, making it difficult to extract the U_{eff} value. Furthermore, the same group reported Fe–Dy heterometallic clusters, such as the "8"-shaped polyanion $[Fe(L)Dy(H_2O)_2Fe_2(B-\alpha-GeW_9O_{34})(GeW_7O_{29})]_2$ (L = trans-1,2-cyclohexanediamine), where the organic ligand coordinates to Fe^{3+}.[144] Magnetic analysis revealed frequency-dependent in-phase (χ'_m) signals and significant out-of-phase (χ''_m) signals indicative of potential single-molecule magnet (SMM) behavior.

In 2023, T. Minato and coworkers reported a cationic glue strategy to form large-sized multinuclear metal encapsulated clusters using SiW_9 building units.[145] This work demonstrated the formation of the $Ln_2Mn_2(FeMn_4)_2$ cluster via the intermediate $FeMn_4$ cluster (Fig. 10a). The multinuclear clusters $\{(FeMn_4)Mn_2Lu_2(FeMn_4)\}$ (II_{Lu}) showed intramolecular ferromagnetic interaction, but these clusters did not show any significant AC magnetic susceptibility under different frequencies and temperatures (Fig. 10b). To reduce the ferromagnetic interaction, the acetate ligands were removed by the addition of acid in acetonitrile solution and formed a $Lu_2Mn_2(FeMn_4)_2$ cluster (III_{Lu}). The octahedral distortion parameter decreases around one of the Mn centers due to the removal of acetate ligands. The cluster shows significant frequency and
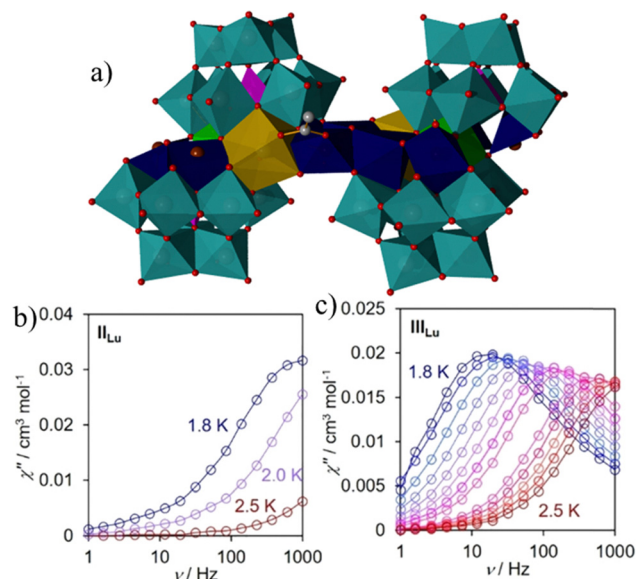

Fig. 10 The molecular structure of III_{Lu} (a), the frequency-dependent out-of-phase magnetic susceptibility plots of II_{Lu} (b) and III_{Lu} (c). Color code: cyan octahedron $\{WO_6\}$, yellow polyhedron Dy unit, blue polyhedron Mn unit, green Fe unit, red O, and grey C. Hydrogen atoms are omitted for clarity. Figures adapted from ref. 145, with permission from Wiley, copyright 2023.

temperature-dependent AC magnetic susceptibility enhancement with an energy barrier of 29.1 K at zero external DC field (Fig. 10c). Finally, a third family of interest involves the functionalization of polyoxotungstates (POTs) by incorporating organic groups, such as organophosphates ($RP^VO_3^{2-}$). Various homometallic organophosphate-functionalized lacunary POTs have been reported, including Keggin-type structures like $[A-\alpha-XW_9(RPO)_2]_5$ (X = P^V, As^V), as well as Wells–Dawson-type complexes such as $[\alpha^2-P_2W_{17}(RPO)2]^{6-}$ and $[P_4W_{24}O_{92}-(C_6H_5PO)_2]^{16-}$.[146–149] In these compounds, the organophosphate P^V centers bind to two oxygen atoms of the POT, one of which is a terminal oxygen atom, while the organic moiety (R) adopts a tetrahedral geometry. This integration combines the inherent properties of the polyanions with the reactive, chiral, and photosensitive characteristics of the organic moieties, resulting in versatile organic–inorganic hybrids. However, comprehensive studies integrating magnetism are currently lacking. One notable example by P. Kogerler and coworkers explored the reactivity of a phenyl phosphonate-decorated mono lacunary Wells–Dawson cluster $[a_2-P^V2\ W_{17}^{VI}O_{61}-(C_6H_5PVO)_2]_6$ ($\{a_2-P_2W_{17}(PhP)_2\}$) with magnetically anisotropic dysprosium(III) ions.[150] The resulting polyanion $[\{(H_2O)_7Dy_2^{III}(a_2, a_{2'}-P_2W_{16}O_{60})(PhPO)_2\}_2]^{8-}$ comprises dimers of bis-lacunary Wells–Dawson-type units $\{a_2,a_{2'}-P_2W_{16}O_{60}\}$ functionalized with both phenyl phosphonate and heterometal (Dy(III)) centers (Fig. 11a and b). Magnetic ac susceptibility data (under an optimal 600 Oe DC field) reveal two distinct slow relaxation processes in different temperature intervals (low-temperature range with $U_{eff} = 17.3\ (\pm2.2)$ K, and higher temperature range with $U_{eff} = 12\ (\pm1.2)$ K) (Fig. 11c).
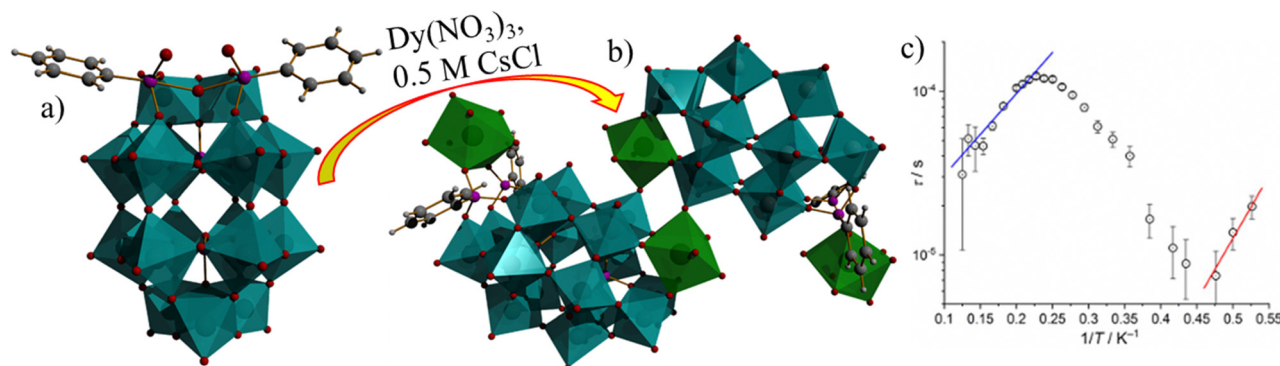
Fig. 11 The structure of the building unit, $[a_2\text{-}P_2W_{17}(PhPO)_2]^{6-}$ (a), the molecular structure of $[\{(H_2O)_7Dy_2\,(a_2,\,a_{2'}\text{-}P_2W_{16}O_{60})(PhPO)_2\}_2]^{8-}$ (b), and magnetic relaxation plot of the complex (c). Color code: cyan octahedron $\{WO_6\}$, green polyhedral Dy, red O, pink P, grey C, white H. Pictures reproduced from ref. 150 with permission from the Royal Society of Chemistry.

Dual heteroatom POT-based SMMs

Heteropolyoxotungstates (HPOTs) represent a promising subclass within the polyoxometalates (POMs) family, valued for their unique electronic properties and spatial geometry. The inclusion of heteroatoms (HAs) in POM building blocks significantly impacts the structural formation and intrinsic properties of these materials.[35,118] In 2018, Cronin and co-workers advanced polyoxometalate chemistry by reporting cross-shaped clusters with different heteroatoms, laying a foundation for the design of new nanoscale molecular architectures.[118] Most lanthanide-containing heteropolyoxometalates (Ln-HPOMs) incorporate a single type of heteroatom. In contrast, those containing two types of heteroatoms are rare due to the differing reactivity and coordination abilities of HAs, making their synthesis challenging. The first dual-HA template HPOT with lanthanides, $[Ln_3Ni_9^{II}(\mu_3\text{-}OH)_9\text{-}(SbW_9O_{33})_2(PW_9O_{34})_3(CH_3COO)_3]^{30-}$ was reported by Kong and co-workers, which included both $[Sb^{III}W_9O_{33}]^{9-}$ and $[P^VW_9O_{34}]^{9-}$ in the same polyanion.[151] More recently, Zhao and co-workers presented the cluster $\{[Ln_4(H_2O)_{18}W_7O_{15}(H_2MA)_4][\alpha\text{-}SbW_9O_{33}]_2\text{-}[HPSbW_{15}O_{54}]_2\}^{20-}$, featuring both Keggin $[\alpha\text{-}SbW_9O_{33}]^{9-}$ and Dawson $[HPSbW_{15}O_{54}]^{11-}$ units.[152] These examples illustrate the potential of utilizing mixed heteroatom templates to design diverse Ln-containing polyoxometalates. In this context, our group has reported two Dy(III)-confined polyoxotungstate complexes

$[Dy_2(H_2O)_7(W_4O_9)(HPSeW_{15}O_{54})(\alpha\text{-}SeW_9O_{33})_2]^{14-}$ (complex **7**) and $\{[Dy_2(H_2O)_{13}W_{14}O_{40}]_2[\alpha\text{-}SeW_9O_{33}]_4[HPSeW_{15}O_{54}]_2\}^{34-}$ (complex **8**) (Fig. 12a and c) using $[HPO_3]^{2-}$ and $[SeO_3]^{2-}$ in the presence of Dy(III) ions.[50] Both complexes exhibit the simultaneous presence of trivacant Keggin $[\alpha\text{-}SeW_9O_{33}]^{8-}$ and Dawson $[HPSeW_{15}O_{54}]^{10-}$ building blocks, incorporating P(III) and Se(IV) heteroatoms. By varying the reaction medium pH and equivalent ratios of the reactant while using the same reactants, we obtained different structural assemblies. Complex **7** consists of a fused structure where two trivacant Keggin $[\alpha\text{-}SeW_9O_{33}]^{8-}$ and Dawson $[HPSeW_{15}O_{54}]^{12-}$ units encapsulate a $[Dy_2(H_2O)(W_4O_9)]^{12+}$ cluster. In contrast, complex **8** comprises four trivacant Keggin and two Dawson units, encapsulating a small cluster of isopolyanions $[Dy_4(H_2O)_{20}W_{14}O_{59}]^{44-}$. Magnetic studies indicate that complex **7** shows slow relaxation of magnetization, with a phenomenological energy barrier of $U_{eff} = 13.58$ K without an external magnetic field (Fig. 12b), which increases to $U_{eff} = 24.57$ K under a 500 Oe dc field. In contrast, complex **8** favors quantum tunneling of magnetization (QTM) in the absence of an external field but demonstrates field-induced slow relaxation of magnetization (1500 Oe applied DC field) with an energy barrier of $U_{eff} = 11.11$ K (Fig. 12d). The observed differences in energy barriers can be attributed to the symmetries and arrangements of the Dy ions within the clusters. The presence of a high symmetry Dy(III) ion

Fig. 12 The molecular structures of $[Dy_2(H_2O)_7(W_4O_9)(HPSeW_{15}O_{54})(\alpha\text{-}SeW_9O_{33})_2]^{14-}$ (a) and $\{[Dy_2(H_2O)_{13}W_{14}O_{40}]_2[\alpha\text{-}SeW_9O_{33}]_4[HPSeW_{15}O_{54}]_2\}^{34-}$ (c)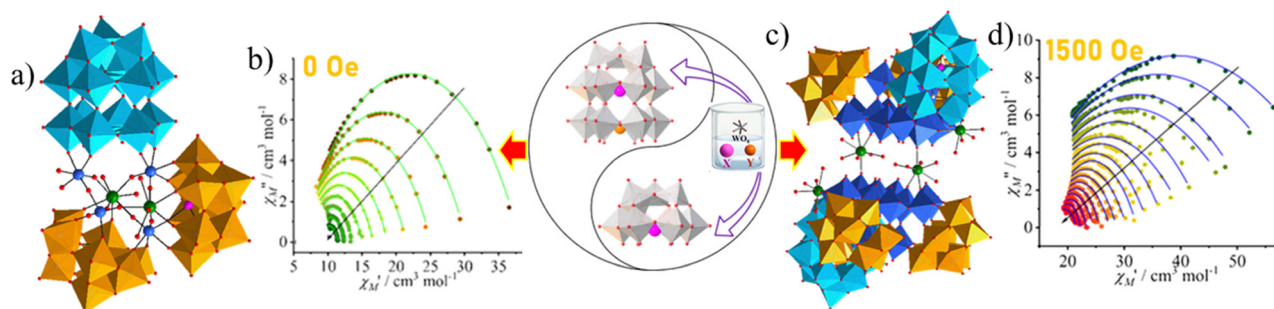. Cole−Cole plot of $[Dy_2(H_2O)_7(W_4O_9)(HPSeW_{15}O_{54})(\alpha\text{-}SeW_9O_{33})_2]^{14-}$ (b) and $\{[Dy_2(H_2O)_{13}W_{14}O_{40}]_2[\alpha\text{-}SeW_9O_{33}]_4[HPSeW_{15}O_{54}]_2\}^{34-}$ (d). Color code: cyan, yellow and blue octahedron $\{WO_6\}$, green Dy, red O, pink P, yellow Se. Figure reprinted (adapted) with permission from ref. 50. Copyright (2024) American Chemical Society.

and a slightly tilted anisotropy axis results in the SMM behavior of complex 7. Although the Dy(III) ions in complex 8 exhibit higher symmetries, their zig-zag arrangement within the cluster reduces the overall anisotropy, thus favoring field-induced single-molecule magnet (SMM) behavior. This marks the first mixed heteroatom-based Dy(III)-substituted polyoxotungstate complex exhibiting single-molecule magnet (SMM) behavior.

Conclusions and future outlook

The increasing fascination with Ln-based POMs undoubtedly stems from the compositional variability of these compounds, which exhibit distinctive chemical and physical properties arising from the synergistic interplay between the POM coordinative structures and Ln(III) constituents. This review succinctly outlines the preparation methods for different types of POTs and provides a thorough summary of how the magnetic properties of these Ln-based POTs are influenced by the coordination symmetry surrounding the Ln-ions.

The synthesis of POT-based Ln-clusters has been challenging due to the easy hydrolysis of Ln(III) ions and the strong reactivity between Ln and POTs, leading to precipitation and difficult crystallization, as well as coordination competition between different metal ions and POTs, especially for high-nuclearity clusters. To overcome these challenges, a mixed strategy integrating inorganic clusters with organic ligands, anionic template methods, and a slow-release strategy of lanthanide ions may be the most effective approach for the synthesis of more POT-based lanthanide oxo clusters (LnOCs).

Nevertheless, as a crucial aspect of magnetism, it is essential to investigate methods for enhancing the thermal energy barrier and the magnetic blocking temperature of LnOCs, which continues to present a formidable challenge. One method to achieve a significant thermal energy barrier in LnOCs involves adjusting the geometry of Ln(III) ions to enhance their axial symmetry. This can be accomplished through the utilization of a monovacant POT unit in conjunction with a moderately flexible electron donor organic ligand. In addition to this, organic–inorganic LnOCs, featuring Ln(III) ions, can impart magnetic properties alongside luminescent characteristics. Furthermore, POMs can contribute redox and catalytic properties,[153,154] and organic co-ligands can add chirality and solubility. Thus, LnOCs offer the potential to combine multiple functionalities within a single molecule.

Future research could also focus on the selective combination of different heteroatoms to construct unusual POM building blocks and enable the design of multi-component lanthanide-based POM derivatives. Combining all component properties in lanthanide-based POMs and studying their effects on magnetic behavior will open new avenues for applications in molecular magnetism.

There is still a long way to go before we can design and manufacture practical Ln-based POMs with unique features, but we should be able to do so in the future and see them used in more research fields.

Data availability

No primary research results, software, or code have been included, and no new data were generated or analyzed as part of this review.

Conflicts of interest

There are no conflicts to declare.

Acknowledgements

References

1 R. Sessoli, H. L. Tsai, A. R. Schake, S. Wang, J. B. Vincent, K. Folting, D. Gatteschi, G. Christou and D. N. Hendrickson, J. Am. Chem. Soc., 1993, 115, 1804–1816.
2 N. Ishikawa, M. Sugita, T. Ishikawa, S.-Y. Koshihara and Y. Kaizu, J. Am. Chem. Soc., 2003, 125, 8694–8695.
3 A. Zabala-Lekuona, J. M. Seco and E. Colacio, Coord. Chem. Rev., 2021, 441, 213984.
4 S. Goswami, A. K. Mondal and S. Konar, Inorg. Chem. Front., 2015, 2, 687–712.
5 L. Bogani and W. Wernsdorfer, Nat. Mater., 2008, 7, 179–186.
6 M. Mannini, F. Pineider, P. Sainctavit, C. Danieli, E. Otero, C. Sciancalepore, A. M. Talarico, M.-A. Arrio, A. Cornia, D. Gatteschi and R. Sessoli, Nat. Mater., 2009, 8, 194–197.
7 M. A. Hay and C. Boskovic, Chem. – Eur. J., 2021, 27, 3608–3637.
8 S. Thiele, F. Balestro, R. Ballou, S. Klyatskaya, M. Ruben and W. Wernsdorfer, Science, 2014, 344, 1135–1138.
9 D. N. Woodruff, R. E. P. Winpenny and R. A. Layfield, Chem. Rev., 2013, 113, 5110–5148.
10 R. Sessoli and A. K. Powell, Coord. Chem. Rev., 2009, 253, 2328–2341.
11 Y.-S. Meng, S.-D. Jiang, B.-W. Wang and S. Gao, Acc. Chem. Res., 2016, 49, 2381–2389.
12 H.-D. Li, S.-G. Wu and M.-L. Tong, Chem. Commun., 2023, 59, 6159–6170.
13 J.-L. Liu, Y.-C. Chen and M.-L. Tong, Chem. Soc. Rev., 2018, 47, 2431–2453.
14 S. G. McAdams, A.-M. Ariciu, A. K. Kostopoulos, J. P. S. Walsh and F. Tuna, Coord. Chem. Rev., 2017, 346, 216–239.
15 P. Kumar Sahu, A. Mondal and S. Konar, Chem. – Eur. J., 2023, 29, e202203664.
16 M. Feng and M.-L. Tong, Chem. – Eur. J., 2018, 24, 7574–7594.
17 P. Kumar Sahu, R. Kharel, S. Shome, S. Goswami and S. Konar, Coord. Chem. Rev., 2023, 475, 214871.
18 Y.-F. Deng, T. Han, B. Yin and Y.-Z. Zheng, Inorg. Chem. Front., 2017, 4, 1141–1148.
19 A. B. Canaj, S. Dey, O. Céspedes, C. Wilson, G. Rajaraman and M. Murrie, Chem. Commun., 2020, 56, 1533–1536.
20 P. K. Sahu and S. Konar, Inorg. Chim. Acta, 2024, 572, 122255.
21 S. T. Liddle and J. V. Slageren, Chem. Soc. Rev., 2015, 44, 6655–6669.
22 P. Zhang, Y.-N. Guo and J. Tang, Coord. Chem. Rev., 2013, 257, 1728–1763.
23 Z. Zhu and J. Tang, Chem. Soc. Rev., 2022, 51, 9469–9481.
24 Z. Zhu and J. Tang, Nat. Sci. Rev., 2022, 9, nwac194.
25 A. Mondal, M. Raizada, P. K. Sahu and S. Konar, Inorg. Chem. Front., 2021, 8, 4625–4633.
26 E. Lowe, C. Wilson, A. B. Canaj and M. Murrie, Dalton Trans., 2025, 54, 477–481.
27 A. Mondal and S. Konar, Chem. – Eur. J., 2021, 27, 3449–3456.
28 A. Mondal and S. Konar, Dalton Trans., 2021, 50, 13666–13670.

29 S. P. Bera, A. Mondal and S. Konar, *Inorg. Chem. Front.*, 2020, **7**, 3352–3363.

30 S. P. Bera, A. Mondal and S. Konar, *Inorg. Chem. Front.*, 2020, **7**, 3352–3363.

31 Y.-C. Chen and M.-L. Tong, *Chem. Sci.*, 2022, **13**, 8716–8726.

32 A. Mondal and S. Konar, *Dalton Trans.*, 2022, **51**, 1464–1473.

33 P. Kumar Sahu and S. Konar, *Chem. – Eur. J.*, 2024, **30**, e202402439.

34 A. Mondal and S. Konar, *Dalton Trans.*, 2022, **51**, 1464–1473.

35 Q. Zheng, M. Kupper, W. Xuan, H. Oki, R. Tsunashima, D.-L. Long and L. Cronin, *J. Am. Chem. Soc.*, 2019, **141**, 13479–13486.

36 A. Paul, S. D. Adhikary, S. Kapurwan and S. Konar, *J. Mater. Chem. A*, 2022, **10**, 13152–13169.

37 L. Cronin and A. Müller, *Chem. Soc. Rev.*, 2012, **41**, 7333–7334.

38 N. I. Gumerova and A. Rompel, *Chem. Soc. Rev.*, 2020, **49**, 7568–7601.

39 E. Coronado and C. J. Gómez-García, *Chem. Rev.*, 1998, **98**, 273–296.

40 P. Ma, R. Wan, Y. Wang, F. Hu, D. Zhang, J. Niu and J. Wang, *Inorg. Chem.*, 2016, **55**, 918–924.

41 A. H. Ismail, B. S. Bassil, G. H. Yassin, B. Keita and U. Kortz, *Chem. – Eur. J.*, 2012, **18**, 6163–6166.

42 J. Goura, B. S. Bassil, X. Ma, A. Rajan, E. Moreno-Pineda, J. Schnack, M. Ibrahim, A. K. Powell, M. Ruben, J. Wang, L. Ruhlmann and U. Kortz, *Chem. – Eur. J.*, 2021, **27**, 15081–15085.

43 K. Fukaya and T. Yamase, *Angew. Chem., Int. Ed.*, 2003, **42**, 654–658.

44 J. M. Clemente-Juan, E. Coronado and A. Gaita-Ariño, *Chem. Soc. Rev.*, 2012, **41**, 7464–7478.

45 Z. Li, X.-X. Li, T. Yang, Z.-W. Cai and S.-T. Zheng, *Angew. Chem., Int. Ed.*, 2017, **56**, 2664–2669.

46 P. K. Sahu, A. Mondal and S. Konar, *Dalton Trans.*, 2021, **50**, 3825–3831.

47 W.-C. Chen, C. Qin, X.-L. Wang, Y.-G. Li, H.-Y. Zang, K.-Z. Shao, Z.-M. Su and E.-B. Wang, *Dalton Trans.*, 2015, **44**, 11290–11293.

48 M. J. Martínez-Pérez, S. Cardona-Serra, C. Schlegel, F. Moro, P. J. Alonso, H. Prima-García, J. M. Clemente-Juan, M. Evangelisti, A. Gaita-Ariño, J. Sesé, J. van Slageren, E. Coronado and F. Luis, *Phys. Rev. Lett.*, 2012, **108**, 247213.

49 M. Shiddiq, D. Komijani, Y. Duan, A. Gaita-Ariño, E. Coronado and S. Hill, *Nature*, 2016, **531**, 348–351.

50 S. Kapurwan, P. K. Sahu and S. Konar, *Inorg. Chem.*, 2024, **63**, 4492–4501.

51 S. Takahashi, I. S. Tupitsyn, J. van Tol, C. C. Beedle, D. N. Hendrickson and P. C. E. Stamp, *Nature*, 2011, **476**, 76–79.

52 J. M. Clemente-Juan and E. Coronado, *Coord. Chem. Rev.*, 1999, **193–195**, 361–394.

53 U. Kortz, A. Müller, J. van Slageren, J. Schnack, N. S. Dalal and M. Dressel, *Coord. Chem. Rev.*, 2009, **253**, 2315–2327.

54 P. Kögerler, B. Tsukerblat and A. Müller, *Dalton Trans.*, 2010, **39**, 21–36.

55 C. Ritchie, A. Ferguson, H. Nojiri, H. N. Miras, Y.-F. Song, D.-L. Long, E. Burkholder, M. Murrie, P. Kögerler, E. K. Brechin and L. Cronin, *Angew. Chem., Int. Ed.*, 2008, **47**, 5609–5612.

56 J.-D. Compain, P. Mialane, A. Dolbecq, I. M. Mbomekallé, J. Marrot, F. Sécheresse, E. Rivière, G. Rogez and W. Wernsdorfer, *Angew. Chem., Int. Ed.*, 2009, **48**, 3077–3081.

57 Z.-M. Zhang, S. Yao, Y.-G. Li, H.-H. Wu, Y.-H. Wang, M. Rouzières, R. Clérac, Z.-M. Su and E.-B. Wang, *Chem. Commun.*, 2013, **49**, 2515–2517.

58 M. Ibrahim, Y. Lan, B. S. Bassil, Y. Xiang, A. Suchopar, A. K. Powell and U. Kortz, *Angew. Chem., Int. Ed.*, 2011, **50**, 4708–4711.

59 J. J. Baldoví, S. Cardona-Serra, A. Gaita-Ariño and E. Coronado, *Adv. Inorg. Chem.*, 2017, **69**, 213–249.

60 K. Y. Monakhov, M. Moors and P. Kögerler, *Adv. Inorg. Chem.*, 2017, **69**, 251–286.

61 C. Ritchie, M. Speldrich, R. W. Gable, L. Sorace, P. Kögerler and C. Boskovic, *Inorg. Chem.*, 2011, **50**, 7004–7014.

62 S. Ghosh, S. Datta, L. Friend, S. Cardona-Serra, A. Gaita-Ariño, E. Coronado and S. Hill, *Dalton Trans.*, 2012, **41**, 13697–13704.

63 M. Vonci, M. J. Giansiracusa, W. Van den Heuvel, R. W. Gable, B. Moubaraki, K. S. Murray, D. Yu, R. A. Mole, A. Soncini and C. Boskovic, *Inorg. Chem.*, 2017, **56**, 378–394.

64 Z.-X. Yang, X.-W. Liang, D. Lin, Q. Zheng and Y. Huo, *Inorg. Chem.*, 2023, **62**, 1466–1475.

65 N. V. Izarova, N. Vankova, A. Banerjee, G. B. Jameson, T. Heine, F. Schinle, O. Hampe and U. Kortz, *Angew. Chem., Int. Ed.*, 2010, **49**, 7807–7811.

66 P. Hermosilla-Ibáñez, P. E. Car, A. Vega, J. Costamagna, F. Caruso, J.-Y. Pivan, E. L. Fur, E. Spodine and D. Venegas-Yazigi, *Cryst. Eng. Commun.*, 2012, **14**, 5604–5612.

67 S. Cardona-Serra, J. M. Clemente-Juan, A. Gaita-Ariño, N. Suaud, O. Svoboda and E. Coronado, *Chem. Commun.*, 2013, **49**, 9621–9623.

68 S. Cardona-Serra, J. M. Clemente-Juan, E. Coronado, A. Gaita-Ariño, N. Suaud, O. Svoboda, R. Bastardis, N. Guihéry and J. J. Palacios, *Chem. – Eur. J.*, 2015, **21**, 763–769.

69 A. Palii, S. Aldoshin, B. Tsukerblat, J. J. Borràs-Almenar, J. M. Clemente-Juan, S. Cardona-Serra and E. Coronado, *Inorg. Chem.*, 2017, **56**, 9547–9554.

70 M. Nicolaou, M. G. Papanikolaou, A. C. Tsipis, T. A. Kabanos, A. D. Keramidas, S. Sproules and H. N. Miras, *Chem. – Eur. J.*, 2018, **24**, 3836–3845.

71 P. Wu, Y. Wang, W. Chen, X. Hu, B. Huang and Z. Xiao, *Inorg. Chem.*, 2021, **60**, 4347–4351.

72 C. M. Granadeiro, D. Julião, S. O. Ribeiro, L. Cunha-Silva and S. S. Balula, *Coord. Chem. Rev.*, 2023, **476**, 214914.

73 Z.-X. Yang, F. Gong, D. Lin and Y. Huo, *Coord. Chem. Rev.*, 2023, **492**, 215205.

74 J.-W. Zhao, Y.-Z. Li, L.-J. Chen and G.-Y. Yang, *Chem. Commun.*, 2016, **52**, 4418–4445.

75 A. Bijelic, M. Aureliano and A. Rompel, *Chem. Commun.*, 2018, **54**, 1153–1169.

76 S.-R. Li, W.-D. Liu, L.-S. Long, L.-S. Zheng and X.-J. Kong, *Polyoxometalates*, 2023, **2**, 9140022.

77 D. Lockey, C. Mathis, H. N. Miras and L. Cronin, *Matter*, 2022, **5**, 302–313.

78 N. L. Bell, M. Kupper and L. Cronin, *Chem. Mater.*, 2021, **33**, 7263–7271.

79 M. T.-K. Ng, N. L. Bell, D.-L. Long and L. Cronin, *J. Am. Chem. Soc.*, 2021, **143**, 20059–20063.

80 S. She, N. L. Bell, D. Zheng, J. S. Mathieson, M. D. Castro, D.-L. Long, J. Koehnke and L. Cronin, *Chem*, 2022, **8**, 2734–2748.

81 T. Minato, D. Salley, N. Mizuno, K. Yamaguchi, L. Cronin and K. Suzuki, *J. Am. Chem. Soc.*, 2021, **143**, 12809–12816.

82 Y. Chen, F. Li, S. Li, L. Zhang and M. Sun, *Inorg. Chem. Commun.*, 2022, **135**, 109084.

83 Y. Zhou, G. Chen, Z. Long and J. Wang, *RSC Adv.*, 2014, **4**, 42092–42113.

84 D. Wang, L. Liu, J. Jiang, L. Chen and J. Zhao, *Nanoscale*, 2020, **12**, 5705–5718.

85 B. Huang, D.-H. Yang and B.-H. Han, *J. Mater. Chem. A*, 2020, **8**, 4593–4628.

86 N. I. Gumerova and A. Rompel, *Nat. Rev. Chem.*, 2018, **2**, 0112.

87 J. Lehmann, A. Gaita-Ariño, E. Coronado and D. Loss, *Nat. Nanotechnol.*, 2007, **2**, 312–317.

88 D.-L. Long, R. Tsunashima and L. Cronin, *Angew. Chem., Int. Ed.*, 2010, **49**, 1736–1758.

89 M. Ammam, *J. Mater. Chem. A*, 2013, **1**, 6291–6312.

90 Y. Gao, M. Choudhari, G. K. Such and C. Ritchie, *Chem. Sci.*, 2022, **13**, 2510–2527.

91 N. I. Gumerova and A. Rompel, *Sci. Adv.*, 2023, **9**, eadi0814.

92 M. A. AlDamen, J. M. Clemente-Juan, E. Coronado, C. Martí-Gastaldo and A. Gaita-Ariño, *J. Am. Chem. Soc.*, 2008, **130**, 8874–8875.

93 O. Y. Mariichak, S. Kaabel, Y. A. Karpichev, G. M. Rozantsev, S. V. Radio, C. Pichon, H. Bolvin and J.-P. Sutter, *Magnetochemistry*, 2020, **6**, 53.

94 J. Flores Gonzalez, V. Montigaud, V. Dorcet, K. Bernot, B. Le Guennic, F. Pointillart and O. Cador, *Chem. – Eur. J.*, 2021, **27**, 10160–10168.

95 M. Ibrahim, V. Mereacre, N. Leblanc, W. Wernsdorfer, C. E. Anson and A. K. Powell, *Angew. Chem. Int. Ed.*, 2015, **54**, 15574–15578.

96 J. Xiong, Z.-X. Yang, P. Ma, D. Lin, Q. Zheng and Y. Huo, *Inorg. Chem.*, 2021, **60**, 7519–7526.

97 S. Kapurwan, A. Mondal, P. K. Sahu and S. Konar, *Inorg. Chem.*, 2022, **61**, 17459–17468.

98 R. Sato, K. Suzuki, T. Minato, K. Yamaguchi and N. Mizuno, *Inorg. Chem.*, 2016, **55**, 2023–2029.

99 S. Kapurwan, P. K. Sahu and S. Konar, *Cryst. Growth Des.*, 2024, **24**, 6300–6310.

100 E. Tanuhadi, E. Al-Sayed, G. Novitchi, A. Roller, G. Giester and A. Rompel, *Inorg. Chem.*, 2020, **59**, 8461–8467.

101 Y. Huo, Y.-C. Chen, J.-L. Liu, J.-H. Jia, W.-B. Chen, S.-G. Wu and M.-L. Tong, *Dalton Trans.*, 2017, **46**, 16796–16801.

102 S. Kapurwan, P. K. Sahu, M. Raizada, R. Kharel and S. Konar, *Dalton Trans.*, 2023, **52**, 9377–9388.

103 Y. Nakagawa, K. Uehara and N. Mizuno, *Inorg. Chem.*, 2005, **44**, 9068–9075.

104 K. Uehara, T. Taketsugu, K. Yonehara and N. Mizuno, *Inorg. Chem.*, 2013, **52**, 1133–1140.

105 L.-X. Shi, W.-F. Zhao, X. Xu, J. Tang and C.-D. Wu, *Inorg. Chem.*, 2011, **50**, 12387–12389.

106 E. Ruiz-Bilbao, A. Iturrospe, S. Reinoso, B. Artetxe, G. Beobide, L. San Felices, L. Lezama, J. M. Gutiérrez-Zorrilla, S. Darwish, D. Sensharma and M. J. Zaworotko, *Angew. Chem., Int. Ed.*, 2023, **62**, e202307436.

107 K. Suzuki, R. Sato and N. Mizuno, *Chem. Sci.*, 2013, **4**, 596–600.

108 R. Sato, K. Suzuki, M. Sugawa and N. Mizuno, *Chem. – Eur. J.*, 2013, **19**, 12982–12990.

109 K.-Y. Wang, B. S. Bassil, Z. Lin, I. Römer, S. Vanhaecht, T. N. Parac-Vogt, C. Sáenz de Pipaón, J. R. Galán-Mascarós, L. Fan, J. Cao and U. Kortz, *Chem. – Eur. J.*, 2015, **21**, 18168–18176.

110 Y.-J. Wang, S.-Y. Wu, Y.-Q. Sun, X.-X. Li and S.-T. Zheng, *Chem. Commun.*, 2019, **55**, 2857–2860.

111 L.-Z. Han, C.-Q. Jiao, W.-C. Chen, K.-Z. Shao, L.-Y. Jin and Z.-M. Su, *Dalton Trans.*, 2021, **50**, 11535–11541.

112 P. Mialane, L. Lisnard, A. Mallard, J. Marrot, E. Antic-Fidancev, P. Aschehoug, D. Vivien and F. Sécheresse, *Inorg. Chem.*, 2003, **42**, 2102–2108.

113 M. A. AlDamen, S. Cardona-Serra, J. M. Clemente-Juan, E. Coronado, A. Gaita-Ariño, C. Martí-Gastaldo, F. Luis and O. Montero, *Inorg. Chem.*, 2009, **48**, 3467–3479.

114 A. S. Mougharbel, S. Bhattacharya, B. S. Bassil, A. Rubab, J. van Leusen, P. Kögerler, J. Wojciechowski and U. Kortz, *Inorg. Chem.*, 2020, **59**, 4340–4348.

115 M. Ibrahim, I. M. Mbomekallé, P. de Oliveira, A. Baksi, A. B. Carter, Y. Peng, T. Bergfeldt, S. Malik and C. E. Anson, *ACS Omega*, 2019, **4**, 21873–21882.

116 Y. Huo, Y.-C. Chen, S.-G. Wu, J.-L. Liu, J.-H. Jia, W.-B. Chen, B.-L. Wang, Y.-Q. Zhang and M.-L. Tong, *Inorg. Chem.*, 2019, **58**, 1301–1308.

117 M. H. Alizadeh, S. P. Harmalker, Y. Jeannin, J. Martin-Frere and M. T. Pope, *J. Am. Chem. Soc.*, 1985, **107**, 2662–2669.

118 Q. Zheng, L. Vilà-Nadal, Z. Lang, J.-J. Chen, D.-L. Long, J. S. Mathieson, J. M. Poblet and L. Cronin, *J. Am. Chem. Soc.*, 2018, **140**, 2595–2601.

119 J. A. Fernández, X. López, C. Bo, C. de Graaf, E. J. Baerends and J. M. Poblet, *J. Am. Chem. Soc.*, 2007, **129**, 12244–12253.

120 S. G. Mitchell, T. Boyd, H. N. Miras, D.-L. Long and L. Cronin, *Inorg. Chem.*, 2011, **50**, 136–143.

121 C.-H. Zhan, R. S. Winter, Q. Zheng, J. Yan, J. M. Cameron, D.-L. Long and L. Cronin, *Angew. Chem., Int. Ed.*, 2015, **54**, 14308–14312.

122 M. Stuckart, N. V. Izarova, M. Glöß, J. Klose, C. Schmitz-Antoniak, P. Kögerler, B. Kersting and K. Y. Monakhov, *Inorg. Chem.*, 2021, **60**, 8437–8441.

123 T. Iftikhar, N. V. Izarova, J. van Leusen and P. Kögerler, *Chem. – Eur. J.*, 2021, **27**, 8500–8508.

124 M. Zhu, T. Iwano, M. Tan, D. Akutsu, S. Uchida, G. Chen and X. Fang, *Angew. Chem., Int. Ed.*, 2022, **61**, e202200666.

125 Y.-L. Wu, X.-X. Li, Y.-J. Qi, H. Yu, L. Jin and S.-T. Zheng, *Angew. Chem., Int. Ed.*, 2018, **57**, 8572–8576.

126 S. Cardona-Serra, J. M. Clemente-Juan, E. Coronado, A. Gaita-Ariño, A. Camón, M. Evangelisti, F. Luis, M. J. Martínez-Pérez and J. Sesé, *J. Am. Chem. Soc.*, 2012, **134**, 14982–14990.

127 T. Iftikhar, N. V. Izarova, J. van Leusen and P. Kögerler, *Chem. – Eur. J.*, 2021, **27**, 13376–13383.

128 W. Guan, G. Wang, B. Li and L. Wu, *Coord. Chem. Rev.*, 2023, **481**, 215039.

129 W. Cañon-Mancisidor, G. Paredes-Castillo, P. Hermosilla-Ibáñez, D. Venegas-Yazigi, O. Cador, B. Le Guennic and F. Pointillart, *Eur. J. Inorg. Chem.*, 2021, 4596–4609.

130 S. Reinoso, *Dalton Trans.*, 2011, **40**, 6610–6615.

131 J. Wang, W. Shi, S. Li, Q. Mao, P. Ma, J. Niu and J. Wang, *Dalton Trans.*, 2018, **47**, 7949–7955.

132 H. An, Z. Han and T. Xu, *Inorg. Chem.*, 2010, **49**, 11403–11414.

133 X.-M. Luo, N.-F. Li, Z.-B. Hu, J.-P. Cao, C.-H. Cui, Q.-F. Lin and Y. Xu, *Inorg. Chem.*, 2019, **58**, 2463–2470.

134 C. Ritchie, M. Speldrich, R. W. Gable, L. Sorace, P. Kögerler and C. Boskovic, *Inorg. Chem.*, 2011, **50**, 7004–7014.

135 P. Ma, F. Hu, R. Wan, Y. Huo, D. Zhang, J. Niu and J. Wang, *J. Mater. Chem. C*, 2016, **4**, 5424–5433.

136 Y. Huo, R. Wan, P. Ma, J. Liu, Y. Chen, D. Li, J. Niu, J. Wang and M.-L. Tong, *Inorg. Chem.*, 2017, **56**, 12687–12691.

137 Y. Huo, Y.-C. Chen, S.-G. Wu, J.-H. Jia, W.-B. Chen, J.-L. Liu and M.-L. Tong, *Inorg. Chem.*, 2018, **57**, 6773–6777.

138 H. Kong, Z.-Y. Ruan, Y.-C. Chen, W. Deng, P.-Y. Liao, S.-G. Wu and M.-L. Tong, *Inorg. Chem.*, 2024, **63**, 15964–15972.

139 I. Werner, J. Griebel, A. Masip-Sánchez, X. López, K. Załęski, P. Kozłowski, A. Kahnt, M. Boerner, Z. Warneke, J. Warneke and K. Y. Monakhov, *Inorg. Chem.*, 2023, **62**, 3761–3775.

140 Y. Jiao, S. Sanz, N. V. Izarova, J. van Leusen, S. Sarwar, S. J. Dalgarno, E. K. Brechin and P. Kögerler, *Dalton Trans.*, 2022, **51**, 5409–5413.

141 E. Ruiz-Bilbao, M. Pardo-Almanza, I. Oyarzabal, B. Artetxe, L. S. Felices, J. A. García, J. M. Seco, E. Colacio, L. Lezama and J. M. Gutiérrez-Zorrilla, *Inorg. Chem.*, 2022, **61**, 2428–2443.

142 S. Sarwar, S. Sanz, J. van Leusen, G. S. Nichol, E. K. Brechin and P. Kögerler, *Dalton Trans.*, 2020, **49**, 16638–16642.

143 Y.-N. Gu, D. Zhao, H. Yu, R. Ge, Z. Li, C.-B. Tian, X.-X. Li, Y.-Q. Sun and S.-T. Zheng, *RSC Adv.*, 2019, **9**, 13543–13549.

144 S.-Y. Wu, Y.-J. Wang, J.-X. Jing, X.-X. Li, Y.-Q. Sun and S.-T. Zheng, *Inorg. Chem. Front.*, 2020, **7**, 498–504.

145 T. Minato and M. Sadakane, *Angew. Chem. Int. Ed.*, 2023, **62**, e202309469.

146 X. Yi, N. V. Izarova and P. Kögerler, *Chem. Commun.*, 2018, **54**, 2216–2219.

147 A. V. Anyushin, A. Kondinski and T. N. Parac-Vogt, *Chem. Soc. Rev.*, 2020, **49**, 382–432.

148 E. Hampson, J. M. Cameron, S. Amin, J. Kyo, J. A. Watts, H. Oshio and G. N. Newton, *Angew. Chem., Int. Ed.*, 2019, **58**, 18281–18285.

149 J. M. Cameron, S. Fujimoto, K. Kastner, R-J. Wei, D. Robinson, V. Sans, G. N. Newton and H. H. Oshio, *Chem. – Eur. J.*, 2017, **23**, 47–50.

150 W. Wang, N. V. Izarova, J. van Leusen and P. Kögerler, *Chem. Commun.*, 2020, **56**, 14857–14860.

151 J. Cai, X.-Y. Zheng, J. Xie, Z.-H. Yan, X.-J. Kong, Y.-P. Ren, L.-S. Long and L.-S. Zheng, *Inorg. Chem.*, 2017, **56**, 8439–8445.

152 S. Xie, D. Wang, Z. Wang, J. Liu, L. Chen and J. Zhao, *Inorg. Chem. Front.*, 2022, **9**, 350–362.

153 H. Kong, J.-Y. Wang, J.-C. Liu, L. Zhang, P.-Y. Liao, Y.-Q. Qi, Z. Liu, S.-G. Wu and M.-L. Tong, *Angew. Chem. Int. Ed.*, 2025, e202422557.

154 D.-H. Li, X.-Y. Zhang, J.-Q. Lv, P.-W. Cai, Y.-Q. Sun, C. Sun and S.-T. Zheng, *Angew. Chem. Int. Ed.*, 2023, **62**, e202312706.